

Tombusvirus Y-Shaped Translational Enhancer Forms a Complex with eIF4F and Can Be Functionally Replaced by Heterologous Translational Enhancers

Beth L. Nicholson,^a Olga Zaslaver,^a Laura K. Mayberry,^b Karen S. Browning,^b K. Andrew White^a

Department of Biology, York University, Toronto, Ontario, Canada^a; Department of Chemistry and Biochemistry and the Institute for Cellular and Molecular Biology, University of Texas, Austin, Texas, USA^b

Certain plus-strand RNA plant viruses that are uncapped and nonpolyadenylated rely on RNA elements in their 3' untranslated region, termed 3'-cap-independent translational enhancers (3'CITEs), for efficient translation of their proteins. Here, we have investigated the properties of the Y-shaped class of 3'CITE present in the tombusvirus *Carnation Italian ringspot virus* (CIRV). While some types of 3'CITE have been found to function through recruitment of translation initiation factors to the viral genome, no *trans*-acting translation-related factors have yet been identified for the Y-shaped 3'CITE. Our results indicate that the CIRV 3'CITE complexes with eIF4F and eIFiso4F, with the former mediating translation more efficiently than the latter. In nature, some classes of 3'CITE are present in several different viral genera, suggesting that these elements hold a high degree of modularity. Here, we test this concept by engineering chimeric viruses containing heterologous 3'CITEs and show that the Y-shaped class of 3'CITE in CIRV can be replaced by two alternative types of 3'CITE, i.e., a *Panicum mosaic virus*-like 3'CITE or an I-shaped 3'CITE, without any major loss in *in vitro* translation or replication efficiency in protoplasts. The heterologous 3'CITEs also mediated whole-plant infections of *Nicotiana benthamiana*, where distinct symptoms were observed for each of the alternative 3'CITEs and 3'CITE evolution occurred during serial passaging. Our results supply new information on Y-shaped 3'CITE function and provide insights into 3'CITE virus-host compatibilities.

Immediately after a plus-strand RNA virus enters a host cell and uncoats, ribosomes are recruited to its genome for translation of viral proteins. The genomic RNA must be a highly efficient template for translation in order to effectively compete with cellular messenger RNAs for the translation machinery. Eukaryotic mRNAs contain specialized structures for ribosome recruitment, namely, a 5' m⁷G cap and a 3' poly(A) tail, which act synergistically to enhance translation (1). Eukaryotic initiation factor 4F (eIF4F) binds directly to the 5' cap through its eIF4E subunit, while the poly(A) tail is bound by poly(A)-binding protein (PABP) (2). eIF4G, the large subunit of eIF4F, binds simultaneously to eIF4E and PABP (3), thereby forming a protein bridge between the two terminal structures and circularizing the mRNA (4). eIF4G also binds eIF3, which recruits the 40S subunit of the ribosome (5). In plants, ribosome recruitment to an mRNA can also be facilitated by an eIF4F isoform, eIFiso4F, which contains its own distinct eIFiso4E and eIFiso4G subunits (6).

Many plus-strand RNA plant viruses do not contain a 5' cap or 3' poly(A) tail and must therefore recruit the host translational apparatus via other mechanisms (7). For some uncapped and nonpolyadenylated RNA plant viruses, this involves translation enhancer elements located in or near the 3' untranslated region (3'UTR) that are essential for viral translation (8). These 3'-cap-independent translation enhancers (3'CITEs) have diverse structures and binding activities, and these differences have allowed their grouping into several major classes (8, 9).

Viruses of the luteovirus genus *Barley yellow dwarf virus* (BYDV) contain a compact, cruciform 3'CITE (10), and versions of it, termed BYDV-like 3'CITEs (BTEs), have been identified in several other viruses (11, 12), including *Tobacco necrosis virus* strain D (TNV-D) (13) (Table 1 and Fig. 1E). The *Panicum mosaic virus* (PMV)-like 3'CITE (PTE), first identified in PMV (14) and

also found in the aureusvirus *Cucumber leaf spot virus* (CLSV) (Table 1 and Fig. 1D), forms a compact tertiary structure involving a pseudoknot between a G-rich bulge and a C-rich sequence (15). The smallest 3'CITE identified so far is the I-shaped class first identified in the tombusvirus *Maize necrotic streak virus* (MNeSV) (16) (Fig. 1C). The I-shaped 3'CITE is also present in some aureusviruses and carmoviruses (17, 18) (Table 1) and contains a highly conserved internal loop motif within an extended stem-loop structure (17). Other tombusviruses, including *Tomato bushy stunt virus* (TBSV) and *Carnation Italian ringspot virus* (CIRV), contain the large Y-shaped 3'CITE (19, 20, 21) (Table 1 and Fig. 1A and B).

Despite considerable diversity in sequence and structure, many 3'CITEs appear to facilitate translation through a similar general mechanism that includes (i) recruitment of components of the translational machinery to the 3'CITE, (ii) interaction between the 3'CITE and 5'UTR, and (iii) 5'-end-dependent ribosome entry onto the viral genome. In fact, the BTE, PTE, and I-shaped 3'CITEs have all been shown to bind to one or more subunits of the eIF4F complex (17, 22, 23); however, the potential host factors that interact with the Y-shaped 3'CITE remain unknown.

Recruitment of eIF4F to the 3' end of the genome, rather than the 5' end where translation initiates, necessitates communication between the 3'CITE and the 5'UTR. For most 3'CITEs, this is

Received 28 September 2012 Accepted 21 November 2012

Published ahead of print 28 November 2012

Address correspondence to K. Andrew White, kawhite@yorku.ca.

Copyright © 2013, American Society for Microbiology. All Rights Reserved.

doi:10.1128/JVI.02711-12

TABLE 1 Phylogenetic distribution of Y-shaped, I-shaped, PTE, and BTE 3'CITEs

3'CITE class and genus ^a			
Y shaped	I shaped	PTE	BTE
Tombusvirus (dicot infecting)	Tombusvirus (monocot infecting)	Panicovirus	Luteovirus
	Carmovirus	Umbravirus	Umbravirus
	Aureusvirus	Aureusvirus	Necrovirus
		Carmovirus	Dianthovirus

^a The column heads identify the four different classes of 3'CITE contained in the wt and hybrid genomes used in this study. The bottom rows list the genera that contain viruses naturally harboring each type of 3'CITE. The genera of origin for the specific 3'CITEs engineered into hybrid CIRV genomes are shown in bold, and the predicted secondary structures of these elements are shown in Fig. 1.

achieved through a long-distance RNA-RNA base-pairing interaction between complementary adapter sequences in the 3'CITE and 5'UTR (17, 19, 20, 24, 25). Recent evidence supports a model in which the 3'-5' interaction allows the 3'CITE-bound eIF4F to recruit the 40S ribosomal subunit to the 5' end of the genome, where it enters and begins scanning (17, 20, 26). In contrast, the T-shaped structure (TSS) class of 3'CITE found in carmoviruses and umbraviruses employs an alternative mechanism, which involves direct recruitment of the ribosome and possible ribosome-mediated colocalization of 3'CITE and 5'UTR (27, 28).

Interestingly, the phylogenetic distribution of the different classes of 3'CITE does not correlate with virus taxonomic classification (9). For example, viruses containing a BTE are present in four different genera spanning at least two families (12). Furthermore, different classes of 3'CITE are often present within a single genus (9). This eclectic distribution of 3'CITEs suggests that they have been exchanged between viruses through genomic RNA-RNA recombination (29). In this scenario, 3'CITEs would represent interchangeable modules able to function effectively in the context of a heterologous viral genome.

The purpose of this study was 2-fold. The first goal was to identify potential host factors that are sequestered by the Y-shaped 3'CITE, and the second objective was to explore the concept of 3'CITE interchangeability through the use of engineered CIRV genomes containing heterologous 3'CITEs. We determined that the CIRV 3'CITE interacts with eIF4F and its isoform and that these factors facilitate translation efficiency. Regarding 3'CITE compatibility, we found that the I-shaped and PTE 3'CITEs, but not the BTE, functioned well in place of the wild-type (wt) Y-shaped 3'CITE in CIRV and affected both host range and symptomatology.

MATERIALS AND METHODS

Computer-aided analysis of RNA. The genome sequences of MNeSV (NC_007729), CLSV (EU127904), TNV-D (D00942), *Maize white line mosaic virus* (MWLMV) (NC_009533), *Johnsongrass chlorotic stripe mosaic virus* (JCSMV) (NC_005287), *Cucumber Bulgarian virus* (CBV) (NC_004725), and *Melon necrotic spot virus* strain 264 (MNSV-264) (AY330700) were obtained from the NCBI GenBank database. RNA secondary structures were predicted at 37°C using Mfold version 3.5 (30, 31).

Plasmid construction and mutagenesis. The infectious full-length clone of CIRV has been described previously (32). CIRV-M was made by substituting nucleotides 4410 to 4673 of the CIRV genome with nucleotides 3892 to 4003 from MNeSV. Similarly, CIRV-C and CIRV-T contain nucleotides 4196 to 4319 from CLSV and 3506 to 3660 from TNV-D,

respectively, in place of nucleotides 4427 to 4655 in the CIRV genome. All mutations to the wt and hybrid CIRV genomes were made through oligonucleotide-mediated PCR-based mutagenesis and standard cloning techniques (33). The PCR-derived regions of all constructs were sequenced to ensure that only the desired sequence changes had been introduced. Constructs containing a StreptoTag were generated by PCR amplification of the desired viral sequence with a reverse primer containing the streptomycin aptamer described previously (34), which has the RNA sequence 5'-GGAUCGCAUUUGGACUUCUGCCCCGCAAGGGCACCACGGUCGGAUCC.

In vitro transcription. DNA plasmids containing a T7 promoter were linearized with *Sma*I and transcribed into RNA using AmpliScribe T7-Flash transcription kits (Epicenter Technologies) as described previously (35).

Protein expression and purification. Native (non-affinity-tagged) versions of eIF4F, eIFiso4F, eIF4G, and eIF4E were expressed and purified as described previously (36).

In vitro translation. Subsaturating concentrations (25 nM) of *in vitro*-generated transcripts were translated in nuclease-treated wheat germ extract (wge) (Promega) in the presence of [³⁵S]methionine ([³⁵S]met), as described previously (21). Reaction mixtures contained 130 mM KOAc and 2.1 mM MgOAc, and the total reaction volume was 20 µl. Protein products were separated by SDS-PAGE in 12% polyacrylamide gels and quantified by radioanalytical scanning of the gels using a PhosphorImager Plus Molecular Imager (Bio-Rad) and QuantityOne software (Bio-Rad). Each experiment was performed at least three times. Cap-binding factor-depleted wge used for translation assays was generated by incubation with 7-methyl GTP-Sepharose 4B (GE Healthcare) and supplemented with purified factors as described previously (37).

StreptoTag affinity chromatography. Preparation of streptomycin-conjugated Sepharose matrix and StreptoTag affinity chromatography were performed as described previously (17, 38). Briefly, StreptoTagged RNA was applied to a 3-ml column of streptomycin-conjugated Sepharose matrix equilibrated with column buffer (50 mM Tris-HCl at pH 7.5, 5 mM MgCl₂, 250 mM NaCl) and incubated at room temperature for 30 min, followed by 3 washes with column buffer. Next, 0.4 ml of wge (Promega) in 1.2 ml of column buffer was applied to the column at 4°C in two 0.8-ml batches, with a 30-min incubation at 4°C after application of each batch. The column was then washed 5 times with column buffer, and RNA-protein complexes were eluted using 1 mM streptomycin. Western blotting of the samples was performed using antisera to eIF4E, eIF4G, eIFiso4E, and eIFiso4G and visualized using a goat anti-rabbit IgG secondary antibody conjugated to horseradish peroxidase (Sigma) and ECL Plus Western blotting detection reagents (Amersham).

Protoplast transfection and viral RNA analysis. Protoplasts were prepared and transfected essentially as described before (35). Briefly, the lower epidermis was removed from 6-to-7-day-old cucumber cotyledons, ~3-week-old *Nicotiana benthamiana* plants (upper leaves), or 5-to-6-day-old barley cotyledons, followed by incubation in cellulase (4 h for cucumber, 90 min for *N. benthamiana* and barley). Protoplasts were then isolated and transfected with viral RNA transcripts (3 µg RNA, 3 × 10⁵ protoplasts) and incubated under conditions of constant fluorescent lighting at 22°C for 22 h. Following incubation, total RNA was extracted from the cells, and accumulation of viral RNA was analyzed by standard Northern blotting using CIRV-specific DNA probes that were end labeled with ³²P. Each experiment was performed at least three times.

Inoculation of *N. benthamiana* plants and RNA analysis. Eight micrograms of *in vitro*-transcribed RNA in a total volume of 10 µl was mixed with an equal volume of GKP buffer (50 mM glycine; 30 mM K₂HPO₄, pH 9.2; 1% bentonite; 1% celite) and used to rub-inoculate two leaves from an approximately 3-week-old *N. benthamiana* plant. Plants were then incubated at 24°C with a 14-h day/10-h night cycle and visually inspected for development of symptoms. Each viral genome was used to inoculate two plants per experiment, and each experiment was performed at least three times. Total nucleic acid extraction from inoculated and upper noninocu-

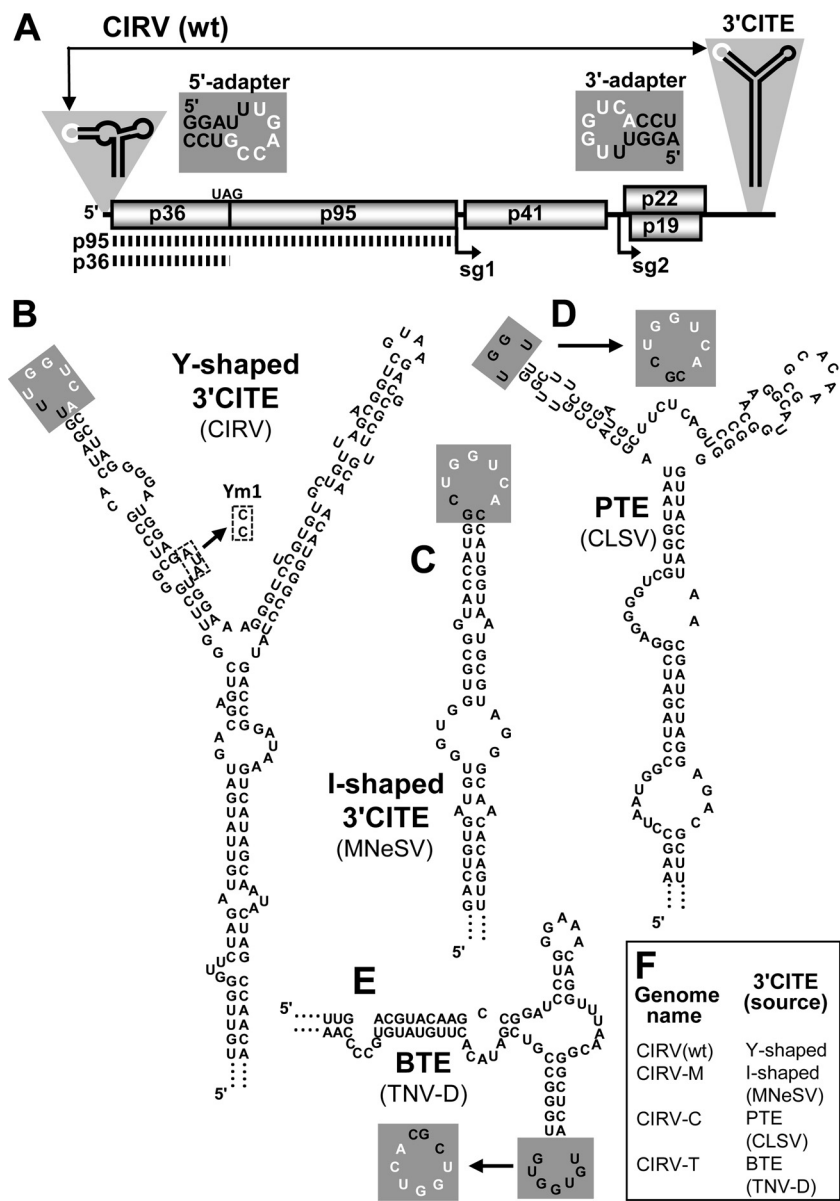


FIG 1 Predicted secondary structures of the CIRV wt and heterologous 3' CITEs used in this study. (A) Schematic representation of the CIRV genome. The thick horizontal line represents the RNA genome, with boxes depicting encoded proteins. Viral protein p36 and its readthrough product p95 are translated directly from the genome, as indicated by the dotted lines below. The start sites of two subgenomic RNAs produced during infection (sg1 and sg2) are shown by arrows below the genome. Sg1 is the template for p41 translation, while p22 and p19 are translated from sg2. The relevant RNA secondary structures in the 5'- and 3'UTRs are depicted schematically, with complementary adapter loops shown in white. The nucleotide sequences of the 5'- and 3'-adapter loops are shown adjacent to the UTRs with black characters in gray boxes, with complementary bases in white. (B) Mfold-predicted Y-shaped secondary structure of the wt CIRV 3' CITE. The 3'-adapter loop is shaded in gray, and bases that are complementary to the 5' adapter are shown in white. The dashed boxes denote the nucleotide substitutions made in mutant Ym1. (C to E) Mfold-predicted secondary structures of the I-shaped-, PTE-, and BTE-class 3' CITEs that were engineered to replace the wt element in the CIRV genome. The virus that naturally contains each 3' CITE is specified alongside the predicted structure. In the PTE (D) and BTE (E), the wt adapter loops (shown in gray boxes) were replaced with the sequence indicated by the arrows to increase base-pairing potential with the CIRV 5'-adapter loop. (F) List of wt and hybrid CIRV genomes used in this study and the wt and heterologous 3' CITEs they contain.

lated leaves was achieved by grinding the leaf tissue in a one-to-one mixture of RNA extraction buffer (100 mM Tris [pH 8.0], 5 mM Na₂EDTA, 200 mM NaCl, 1% SDS) and phenol:chloroform:isoamyl alcohol (PCI) (25:24:1), followed by two additional PCI extractions and ethanol precipitation in the presence of 0.6 M ammonium acetate. Total nucleic acid was separated in 1.4% agarose gels and then transferred to membranes for Northern blot analysis of viral RNA accumulation. The gels were stained with ethidium bromide prior to transfer to ensure uniform loading of samples.

Serial passaging and RNA sequence analysis. Ten microliters of total nucleic acid isolated from the leaves of initially infected plants was used for inoculation of passage-1 plants. Given that CIRV-M did not spread to systemic leaves in initial infections, total nucleic acid from inoculated leaves was used for the first passage. For CIRV-C, nucleic acid from upper noninoculated leaves showing symptoms was used for the first passage. The samples were added to 10 μl of GKP buffer and used for inoculation of *N. benthamiana* plants as described above. For both CIRV-M and CIRV-C, the passage-1 plants developed signs of systemic infection. Ac-

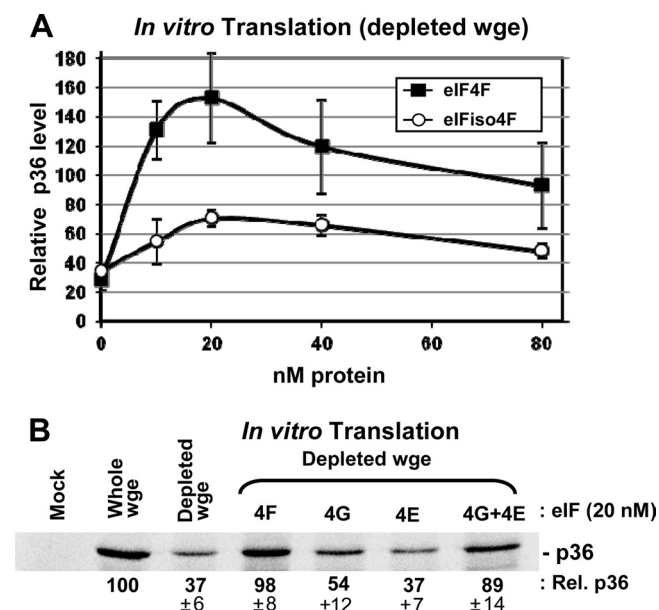


FIG 2 CIRV 3'CITE activity in eIF-depleted wheat germ extract supplemented with eIFs. CIRV genomic RNA was generated *in vitro* and then incubated at a concentration of 25 nM in wge reaction mixtures containing [³⁵S]met for 1 h at 25°C. After separation of proteins by SDS-PAGE, bands corresponding to p36 were quantified by radioanalytical scanning of the gel and normalized to the level of p36 produced in nondepleted wge, which was set at 100. (A) Translation of p36 from CIRV genome RNA in factor-depleted wge supplemented with the indicated amounts of eIF4F or eIFiso4F. Error bars indicate standard errors of the means (SEM) of the results from three separate experiments. (B) SDS-PAGE gel showing p36 accumulation (± SEM) in factor-depleted wge supplemented with 20 nM eIF4F or its subunits as indicated above the gel.

cordingly, RNA was extracted from upper noninoculated leaves showing symptoms and used for the second passage. This process was repeated once more for a total of three serial passages. Total nucleic acid was extracted from noninoculated leaves of passage-3 plants, and the cDNA of full-length genomic RNA was amplified by reverse transcription-PCR (RT-PCR). Subsequently, the cDNA was cloned into pUC19 plasmids and the 3' region was sequenced.

RESULTS

Involvement of eIFs in CIRV 3'CITE activity. Our previous studies demonstrated that the addition of free CIRV Y-shaped 3'CITE (or TBSV Y-shaped 3'CITE) to *in vitro* translation reaction mixtures containing the CIRV genome inhibited translation of p36 from the genome in a dose-dependent manner (21). This ability of free 3'CITE to suppress translation in *trans* suggested that this RNA element can sequester a factor(s) required for efficient translation. As eIF4F and eIFiso4F were found to bind to other classes of 3'CITE (17, 22, 23, 39), these factors represented attractive candidates for CIRV 3'CITE binding. To assess their potential importance, a wheat germ extract (wge) was prepared that was depleted of these translation initiation factors by using m⁷G-Sepharose to selectively remove them from the extract (37). Translation of *in vitro* transcripts of the wild-type (wt) CIRV genome in factor-depleted wge was reduced to ~35% the level of normal wge (Fig. 2A). Addition of purified eIFiso4F or eIF4F to the depleted extract induced partial or more than full restoration of p36 translation from the CIRV genome, respectively (Fig. 2A). Interestingly, high concentrations of the factors reduced the levels of en-

hancement, possibly due to their binding to and exhausting the availability of an additional important component in the extract.

The superior enhancement of translation seen with eIF4F prompted us to also assess the contribution of the individual subunits of this bipartite factor. To this end, purified eIF4G or eIF4E subunits were tested individually for their ability to enhance translation in the depleted extract. A small 1.5-fold enhancement was observed for eIF4G, and no enhancement was seen for eIF4E (Fig. 2B). Conversely, the intact eIF4F complex or concurrent addition of both subunits led to ~2.5-fold levels of translational recovery (Fig. 2B). These results indicate that eIF-mediated enhancement is greatest when both subunits are present.

Next, the possibility that the CIRV 3'CITE interacts with eIF4F was investigated by RNA-affinity chromatography. This was accomplished by fusing wt and mutant forms of the CIRV 3'CITE to a streptomycin RNA aptamer, or StreptoTag (38). A streptomycin-conjugated Sepharose column was used to selectively bind the hybrid StreptoTag-3'CITE RNA. Next, wge extract was passed through the column and, following washes, the RNA and bound factors were eluted with free streptomycin. The mutant 3'CITE (Ym1) used as a negative control in this binding assay contained a substitution of AUA in an internal loop with CC (Fig. 1B). This modification was predicted to pair the internal loop without affecting the secondary structure of the rest of the 3'CITE. When this modification was introduced into the 3'CITE in the CIRV genome (CIRV-Ym1), it rendered the 3'CITE inactive, as demonstrated by the inability of this mutant to efficiently translate p36 in wge (Fig. 3A) and the failure of the same mutant to accumulate when transfected into protoplasts (Fig. 3B).

Several different RNAs were tested for interaction with eIF4F or eIFiso4F using the RNA-affinity approach described above. The I-shaped 3'CITE of MNeSV (known to interact with both eIF4F and eIFiso4F) (17) was used as a positive control, whereas the CIRV 3'CITE mutant Ym1 and the CIRV 5'UTR were included as negative controls. Last, the wt CIRV 3'CITE was tested along with the wt Y-shaped 3'CITE from the related tombusvirus TBSV. Following StreptoTag-based purification with each of the different RNA ligands, eluted proteins were separated by SDS-PAGE and Western blot analysis was performed with different anti-eIF antisera (Fig. 3C). Neither the Ym1 mutant 3'CITE nor the CIRV 5'UTR was found to complex with any of the eIFs, whereas the MNeSV 3'CITE formed complexes with components of both eIF4F and eIFiso4F (Fig. 3C). The wt CIRV 3'CITE also complexed with all four eIF components, as did the wt TBSV 3'CITE (Fig. 3C). In an effort to determine if the CIRV 3'CITE interaction observed was direct, StreptoTag affinity assays and electrophoretic mobility shift assays were performed with the 3'CITE and purified eIF4F. Binding was observed for the wt CIRV 3'CITE; however, the mutant 3'CITE Ym1, as well as other nonfunctional 3'CITE mutants, also bound to eIF4F with comparable affinities (data not shown). An effort was also made to detect a direct interaction via UV cross-linking of the CIRV 3'CITE to eIFs in wge; however, this approach proved unsuccessful. Accordingly, it is clear that the CIRV 3'CITE does complex specifically with eIFs in wge (Fig. 3C); however, it remains unclear whether this interaction is direct or indirect.

***In vitro* and *in vivo* activities of CIRV genomes containing heterologous 3'CITEs.** Having identified eIFs as ligands for the CIRV 3'CITE and knowing that other 3'CITEs also function via this strategy, we wondered whether the CIRV 3'CITE could be

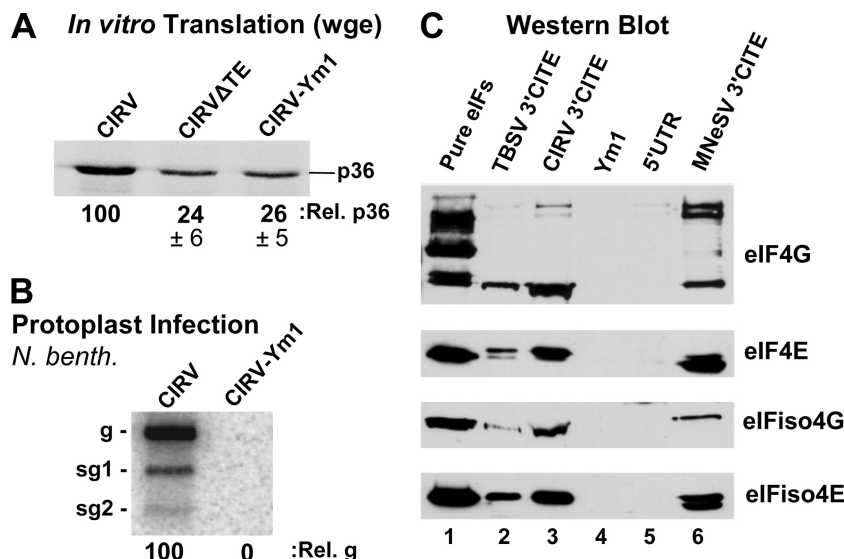


FIG 3 Interaction of the CIRV 3'CITE with eIF4F and eIFiso4F. (A) SDS-PAGE analysis of p36 production in wge. CIRV-ΔTE is a 3'-truncated version of CIRV that does not contain a 3'CITE; CIRV-Ym1 contains a mutated 3'CITE (mutation shown in Fig. 1B). (B) Northern blot showing genomic (g) and subgenomic (sg1 and sg2) viral RNA isolated from cucumber protoplasts 22 h after inoculation with the genomic RNAs indicated above the blot. *N. benth.*, *N. benthamiana*. (C) Western blots showing the detection of the eIFs indicated to the right. Blots were performed on eluates from streptomycin-conjugated Sepharose columns containing StreptoTagged versions of the RNAs indicated above. Prior to elution, columns loaded with RNA were incubated with wge and then washed. Lane 1 contained 2 pmol of each purified eIF; lanes 2 and 3 contained eluate from the wt Y-shaped 3'CITEs of TBSV and CIRV, respectively; lane 4 contained eluate from the CIRV 3'CITE mutant Ym1; lane 5 contained eluate from RNA corresponding to the CIRV 5'UTR; lane 6 contained eluate from the I-shaped 3'CITE of MNeSV, which was used as a positive control.

functionally replaced by different classes of eIF-binding 3'CITE. Previously, we found that a hybrid CIRV genome, generated by replacing the wt Y-shaped 3'CITE of dicot-infecting CIRV with the I-shaped 3'CITE of monocot-infecting MNeSV, was still efficiently translated *in vitro* (17). This result hinted that the different classes of 3'CITE may be interchangeable between viruses. To further investigate this possibility, two additional CIRV genomes containing a heterologous 3'CITE in place of the wt Y-shaped element were constructed (Fig. 1). In addition to CIRV-M, which contains the I-shaped 3'CITE from MNeSV, CIRV-C and CIRV-T were engineered to contain the PTE-class 3'CITE from CLSV and the BTE-class 3'CITE from TNV-D, respectively (Fig. 1C to F). Given that no known tombusviruses naturally contain a PTE- or BTE-class element (Table 1), CIRV-C and CIRV-T represent intergenus 3'CITE exchanges. Since communication between the 3'CITE and 5'UTR is essential for CIRV translation (21), it was important that each heterologous 3'CITE contained an adapter loop sequence that was complementary to the adapter loop in the 5'UTR of CIRV (Fig. 1A). The adapter loop in the wt MNeSV 3'CITE is naturally complementary to the CIRV 5' adapter (Fig. 1A and C) and was previously shown to interact with it (17). However, the natural adapter loops of the CLSV PTE and the TNV-D BTE had less base-pairing potential with the CIRV 5'-adapter sequence and, thus, were replaced with a complementary terminal loop to increase adapter base-pairing potential (Fig. 1D and E).

To assess the viability of the heterologous 3'CITEs in the CIRV genome, *in vitro*-transcribed RNAs of CIRV-M, CIRV-C, and CIRV-T (Fig. 1F) were generated along with wt CIRV and CIRV-ΔTE; the latter contains no 3'CITE due to a 3'-terminal truncation. The viral genomes were then translated *in vitro* in wge in the presence of [³⁵S]methionine, and the accumulation of the p36

auxiliary replication protein (Fig. 1A) was monitored following electrophoresis (Fig. 4A). CIRV-M and CIRV-C were highly active in this assay, mediating 32-fold and 18-fold increases in p36 production, respectively, compared to CIRV-ΔTE (Fig. 4A). The effectiveness of these two chimeric genomes in wge is underscored by the fact that they were translated significantly more efficiently than wt CIRV (Fig. 4A). In contrast, CIRV-T was translated only moderately more efficiently than CIRV-ΔTE, indicating that its BTE activity was weak in this assay (Fig. 4A). Next, the effect of the heterologous 3'CITEs on viral RNA accumulation in plant cells was assessed by transfecting plant protoplasts with the wt or hybrid CIRV genomes and monitoring viral RNA accumulation by Northern blotting (Fig. 4B). In line with the *in vitro* translation data, CIRV-M and CIRV-C accumulated at levels similar to wt CIRV in protoplasts prepared from *Nicotiana benthamiana* plants, while CIRV-T was not detectable (Fig. 4B, upper panel). Similar results were observed when viral RNA accumulation was assessed in protoplasts from barley, a monocotyledonous plant, although CIRV-C levels were ~2.5-fold lower than in the *N. benthamiana* infection (Fig. 4B, compare lower panel with upper panel). Taken together, these results indicate that CIRV genomes containing the heterologous I-shaped or PTE 3'CITEs, but not the BTE, are able to undergo efficient translation *in vitro* and replicate *in vivo* in both dicot and monocot plant protoplasts.

Next, inoculations in *N. benthamiana* plants were performed to determine whether the hybrid CIRV genomes were capable of causing a whole-plant infection. *In vitro*-generated transcripts of wt and hybrid CIRV genomes were rub-inoculated onto leaves, and symptom development was monitored. Within 6 days postinfection (dpi), wt CIRV caused yellowing of the inoculated leaves and viral RNA accumulated to high levels, as detected by Northern blotting (Fig. 5A). CIRV-M caused local infections that induced

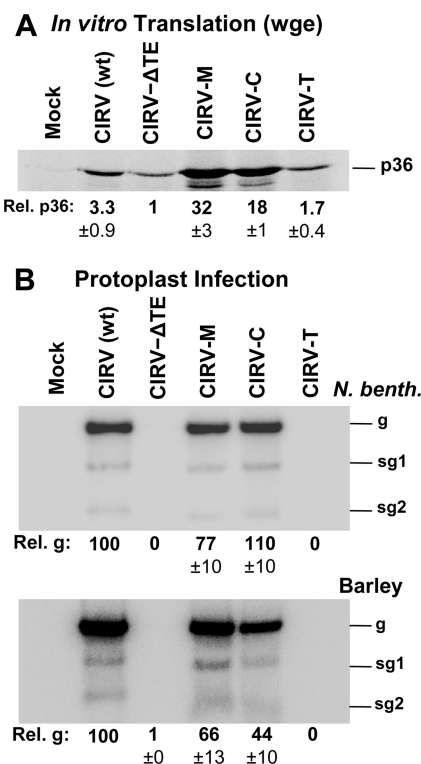


FIG 4 *In vitro* translation and *in vivo* replication of CIRV genomes containing heterologous 3'CITEs. (A) p36 production in wheat germ extract (wge) from wt and hybrid viral genomes. CIRV-M is the hybrid CIRV genome in which the wt Y-shaped 3'CITE was replaced with the I-shaped 3'CITE of MNeSV. Similarly, CIRV-C contains the PTE of CLSV, and CIRV-T contains the BTE of TNV-D. p36 levels are shown below the gel (\pm SEM) relative to CIRV-ΔTE, which was set to 1. (B) Northern blot analysis of viral RNA accumulation in *N. benthamiana* (upper panel) or barley (lower panel) protoplasts inoculated with the RNAs identified at the top. The positions of the genomic (g) and subgenomic (sg1 and sg2) RNAs are indicated to the right of the blots. Relative accumulation of genomic RNA, normalized to wt CIRV (set to 100), is shown below each blot with SEM of the results from three separate experiments.

chlorotic spots on inoculated leaves and the accumulation of viral RNA in inoculated leaf tissue (Fig. 5A). However, the infection did not appear to be as robust as for wt CIRV, as viral RNA accumulated at comparatively lower levels (Fig. 5A). In contrast, CIRV-C consistently caused symptoms of greater severity than wt CIRV infections, including necrosis of the inoculated leaves that was visible as early as 3 dpi (Fig. 5A). Conversely, plants inoculated with CIRV-T did not develop any symptoms or accumulate any detectable viral RNA in inoculated leaves (Fig. 5A). Systemic spread of the viruses was also assessed, using accumulation of viral RNA and development of symptoms in upper noninoculated leaves as indicators. In plants inoculated with wt CIRV, yellowing of noninoculated leaves accompanied by high levels of viral RNA accumulation appeared within 6 dpi (Fig. 5B). Conversely, plants inoculated with CIRV-M showed neither symptoms nor detectable viral RNA in noninoculated leaves (Fig. 5B), indicating that, despite being able to cause a local infection, CIRV-M could not spread systemically in the plant. In contrast, systemic infection of CIRV-C plants, revealed by necrosis of noninoculated leaves and systemic accumulation of viral RNA, consistently occurred within 6 dpi (Fig. 5B). In accordance with the lack of local infection, no signs of systemic infection were detected in plants inoculated with

CIRV-T (Fig. 5B). These whole-plant infection data are in general agreement with the *in vitro* translation and protoplast replication results, in that CIRV-M and CIRV-C caused infection, while CIRV-T did not. Attempts were also made to assess whole-plant infection in barley plants; however, no local or systemic infections were observed with any of the viral genomes tested (data not shown).

Evolution of heterologous 3'CITEs. Having established that the I-shaped and PTE 3'CITEs could functionally replace the Y-shaped 3'CITE *in vitro* and *in vivo*, we next wanted to see whether these RNA elements would adapt to their new genomic context if subjected to serial passage in plants. To this end, total RNA isolated from leaves of initially infected plants was used as an inoculum to start serial passages in *N. benthamiana* plants. Samples from two plants originally inoculated with CIRV-M were used to inoculate passage-1 plants. However, symptoms developed in only one of the two passage-1 plants; therefore, only RNA isolated from this infected plant was carried forward for the second and third passages. For CIRV-C, both passage-1 plants produced severe symptoms and so both were subjected to passage two more times. Viral RNAs isolated after the final passage (passage 3) were converted to cDNA via RT-PCR, and the 3'-terminal 850 nucleotides of the genomes were sequenced and analyzed for changes to the primary sequence of the 3'CITEs. Interestingly, the CIRV-M isolate subjected to passage acquired two G-to-A mutations in the core region of its I-shaped 3'CITE (Fig. 6A), and in the two separate serial passages of CIRV-C, two different mutations involving the same G-U base pair in the PTE were observed (Fig. 6B). In the first CIRV-C isolate (isolate 1), the G-U pair was changed to a G-C base pair through a U-to-C substitution, and in the second isolate (isolate 2), the same G-U pair was changed to an A-U base pair through a G-to-A substitution (Fig. 6B).

We next wanted to determine whether the 3'CITE mutations acquired through serial passage conferred any functional advantage to the hybrid genomes. In order to investigate this, full-length cDNA constructs were made from the genomic RNAs of the passaged CIRV-M isolate and passaged CIRV-C isolate 1, termed CIRV-Mp and CIRV-Cp, respectively (Fig. 6C). However, because it was possible that these clones contained mutations other than those in the 3'CITEs (that could contribute to phenotypic changes), additional genomic constructs were made in which only the 3'CITE mutations that arose during serial passage were introduced into CIRV-M or CIRV-C, termed CIRV-MpTE and CIRV-CpTE, respectively (Fig. 6C). The *in vitro* and *in vivo* activities of these genomes were then assessed in comparison to those of the genomes of CIRV-M and CIRV-C, which contained the original heterologous 3'CITEs (Fig. 7). In wge translation assays, production of p36 from CIRV-Mp and CIRV-MpTE was similar to the level generated by CIRV-M (Fig. 7A). In contrast, *in vitro* translation of CIRV-Cp and CIRV-CpTE was \sim 50% higher than for CIRV-C (Fig. 7A), demonstrating that the single-base change from U to C in the PTE that was selected for during serial passage enhanced its translational activity *in vitro*. When tested in protoplasts, accumulation of CIRV-MpTE showed a small decrease in *N. benthamiana* and small increase in barley relative to CIRV-M accumulation (Fig. 7B). For CIRV-CpTE, minor decreases were observed in both *N. benthamiana* and barley protoplasts relative to CIRV-C (Fig. 7B). Thus, other than a small increase in accumulation in barley protoplasts for CIRV-MpTE, the 3'CITE adapta-

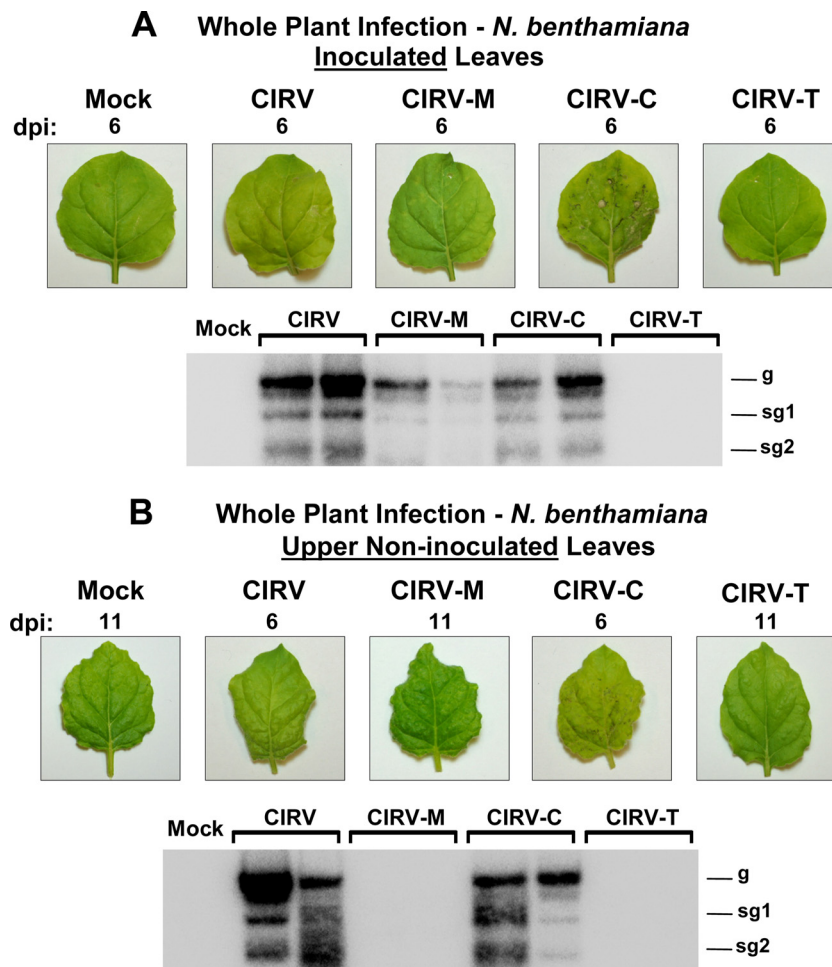


FIG 5 Infection of *N. benthamiana* plants by wt and hybrid CIRV genomes. (A) Upper panel: inoculated leaves 6 days after inoculation with *in vitro*-generated transcripts of the genomes indicated at the top. Lower panel: Northern blot detecting viral RNA extracted 6 days postinoculation (dpi) from leaves inoculated with the genomic RNAs indicated above the blot. The two lanes for each genome contain samples from separate plants. The positions of the genomic (g) and subgenomic (sg1 and sg2) RNAs are shown to the right of the blot. (B) Symptoms (upper panel) and RNA accumulation (lower panel) in upper noninoculated leaves at either 6 dpi (for CIRV and CIRV-C) or 11 dpi (for mock treatment, CIRV-M, and CIRV-T). Leaves shown are representative of all plants inoculated with the indicated genome over three separate experiments. In each trial, two plants were inoculated with each genome.

tions did not appear to confer an accumulation advantage in single-cell infections.

While the two nucleotide substitutions in the I-shaped 3'CITE (Fig. 6A) did not notably augment activity in wge or protoplasts (Fig. 7A and B), they did cause a considerable enhancement of infectivity in whole *N. benthamiana* plants (Fig. 7C). Extensive yellowing and curling of the inoculated leaves were observed in plants infected with CIRV-Mp and CIRV-MpTE but not with CIRV-M (Fig. 7C). Also, the levels of viral RNA extracted from leaves inoculated with CIRV-Mp and CIRV-MpTE were consistently higher than those of viral RNA extracted from CIRV-M-inoculated leaves (Fig. 7C). Moreover, CIRV-Mp and CIRV-MpTE established robust systemic infections of the plants, which CIRV-M was not able to do (Fig. 7C). For plants inoculated with CIRV-Cp and CIRV-CpTE, symptoms were similar to those seen with CIRV-C (Fig. 7C) and viral RNA accumulation in inoculated and noninoculated leaves was somewhat lower than the accumulation seen with CIRV-C (Fig. 7C), indicating that the adaptation in the PTE 3'CITE did not appear to enhance these monitored parameters compared to those of CIRV-C.

A possible alternative conformation for the I-shaped 3'CITE. The secondary structure of the MNeSV I-shaped 3'CITE was previously extensively analyzed by solution structure probing and mutational analysis (17). Mfold analysis of the wild-type MNeSV 3'CITE predicted that it adopts the optimal structure shown in Fig. 8A [1] (17). Interestingly, Mfold analysis of the I-shaped 3'CITE recovered after passage (i.e., containing the two substitutions shown in Fig. 6A) predicted a different optimal structure that included a central stem consisting of four canonical base pairs (Fig. 8A [3]). This difference prompted us to reexamine the secondary structure of the wt MNeSV 3'CITE, as well as other members of the I-shaped class (Fig. 8A). While the wt MNeSV 3'CITE is not predicted by Mfold to form the alternative conformation as its optimal structure, it is possible for it to adopt this suboptimal conformation, albeit with a weaker GU base pair in the central stem (Fig. 8A [2]). Additionally, this alternative conformation is also possible in the I-shaped 3'CITEs of the aureusviruses *Maize white line mosaic virus* (MWLMV) and *Johnsongrass chlorotic stripe mosaic virus* (JCSMV), the tombusvirus *Cucumber Bulgarian virus* (CBV), and the carmovirus *Melon necrotic spot*

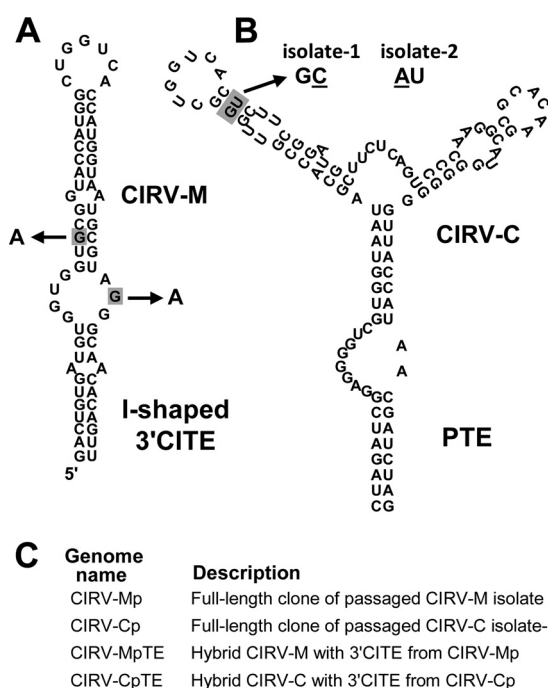


FIG 6 Sequence changes in the I-shaped 3'CITE and PTE acquired during serial passage in plants. (A) Predicted secondary structure of the I-shaped 3'CITE in CIRV-M. The two guanine residues shaded in gray, present in the original 3'CITE of CIRV-M, were substituted with adenine residues during serial passage, as depicted by the arrows. (B) Predicted secondary structure of the PTE in CIRV-C. Changes to the base pair highlighted in gray were observed in two separate serial passage experiments. The single-base substitutions that arose during serial passage in isolate 1 and isolate 2 are shown underlined in the resulting predicted base pairs, indicated above the structure. (C) List of constructs engineered to contain full-length passaged genomes or 3'CITEs containing mutations acquired during passage. See the text for details.

virus strain 264 (MNSV-264) (Fig. 8A, structures [4] to [7]). In fact, these viruses naturally contain the central-stem adenine residue that was acquired by CIRV-M through serial passage (Fig. 8A, structures [4] to [7], asterisks). The alternative conformation for MNSV (Fig. 8A [1]) is also a better fit with the previously reported solution structure data (17). Specifically, two guanine residues previously reported to be highly chemically reactive (17) are positioned in internal loops in the alternative structure, whereas in the optimal Mfold structure one of these guanines is predicted to be base paired (Fig. 8A, compare arrowhead positions in structures [1] and [2]). Based on these observations, we questioned whether the alternative conformation was important for I-shaped 3'CITE function.

A key component of the alternative conformation for the I-shaped 3'CITE is the central four-base-pair helix. In an attempt to assess the functional importance of this stem, different substitutions were introduced at predicted base-paired positions in CIRV-M or CIRV-MpTE that would maintain the stem with different pairing partners (Fig. 8B). The activity of these mutants was then tested in wge translation reactions (Fig. 8C). If formation of the four-base pair stem was important and independent of sequence identity at these positions, then some or all of the alternative base pair substitutions should have been functional. However, all mutants were found to be inactive in wge, except for mutant M3B, which contained the G-to-A mutation that was selected for

by CIRV-M in serial passages (Fig. 8C). Similarly, only the M3B mutant from the group was able to replicate in protoplasts (data not shown). While these results do not provide support for the idea of the importance of this alternative central stem, they also do not conclusively rule out a role for it in which sequence identity of the base pairs is also critical for function. Alternatively, it is possible that both mutually exclusive structures (Fig. 8A [1] and [2]) are required for I-shaped 3'CITE function.

DISCUSSION

Translation of viral proteins is mediated by a 3'CITE in a variety of plus-strand RNA plant viruses that are spread across many genera and at least two plant virus families (8, 9). In the present study, we established an important role for eIF4F in CIRV 3'CITE activity. Additionally, we showed that translation of CIRV can be facilitated by two different heterologous 3'CITEs and that the type of 3'CITE influences both virus-host compatibility and symptomatology in whole-plant infections.

CIRV 3'CITE and eIF4F. Studying the mechanism of function of the Y-shaped 3'CITE in TBSV has been challenging, as the TBSV 3'CITE does not enhance translation from the TBSV genome in wge (40). In fact, of the different Y-shaped 3'CITE-containing tombusviruses tested in wge, only CIRV showed 3'CITE-dependent enhancement of translation (21). This *in vitro* activity allowed us to further pursue the mechanism of function of Y-shaped 3'CITEs using CIRV as a model. On the basis of previous reports of the involvement of eIF4F and its subunits in facilitating 3'CITE activity (9), we investigated whether these factors were also involved in CIRV 3'CITE function. We determined that the CIRV 3'CITE activity is indeed mediated by eIF4F (Fig. 2) and that it interacts with this factor, as well as its isoform, in wge (Fig. 3). As the individual eIF4G and eIF4E subunits did not mediate efficient translation (Fig. 2B), it is likely that the assembled eIF4F complex is required for CIRV 3'CITE function. As several 3'CITEs have been shown to bind directly and specifically to purified eIF4F (17, 23, 39), the lack of specific binding between purified eIF4F and the CIRV 3'CITE was somewhat unexpected. However, results comparable to these were also obtained with the BTE of BYDV (22). For that BTE, those authors proposed that the lack of specificity with the purified factors was due to the requirement of a wge-specific factor/condition or differences in the on/off rates between the wt and mutant 3'CITEs that allowed similar dissociation constants but distinct activities (22). These explanations could also apply to our results with the CIRV 3'CITE; thus, the possibility remains that this 3'CITE may interact directly with eIF4F in order to function. In terms of auxiliary factors, one has been identified for *Red clover necrotic mosaic virus* (RCNMV) (41). For the BTE 3'CITE in the dianthovirus RCNMV (Table 1), poly(A)-binding protein binds to a purine-rich tract upstream from the 3'CITE and mediates eIF4F binding to the 3'CITE (41). In our case, careful inspection of silver-stained gels of the proteins eluted from columns with the wt and mutant CIRV 3'CITEs did not reveal any differentially bound proteins of potential interest (other than eIFiso4G, which was confirmed via mass spectrometry) (data not shown). Accordingly, if a wge-specific factor is required to bridge or facilitate the 3'CITE-eIF4F interaction, higher-resolution methods would be required to identify such factors.

Although it remains to be determined whether eIF4F binding to the CIRV 3'CITE is direct or indirect, formation of this interaction would locate these eIFs proximal to the 3' end of the viral

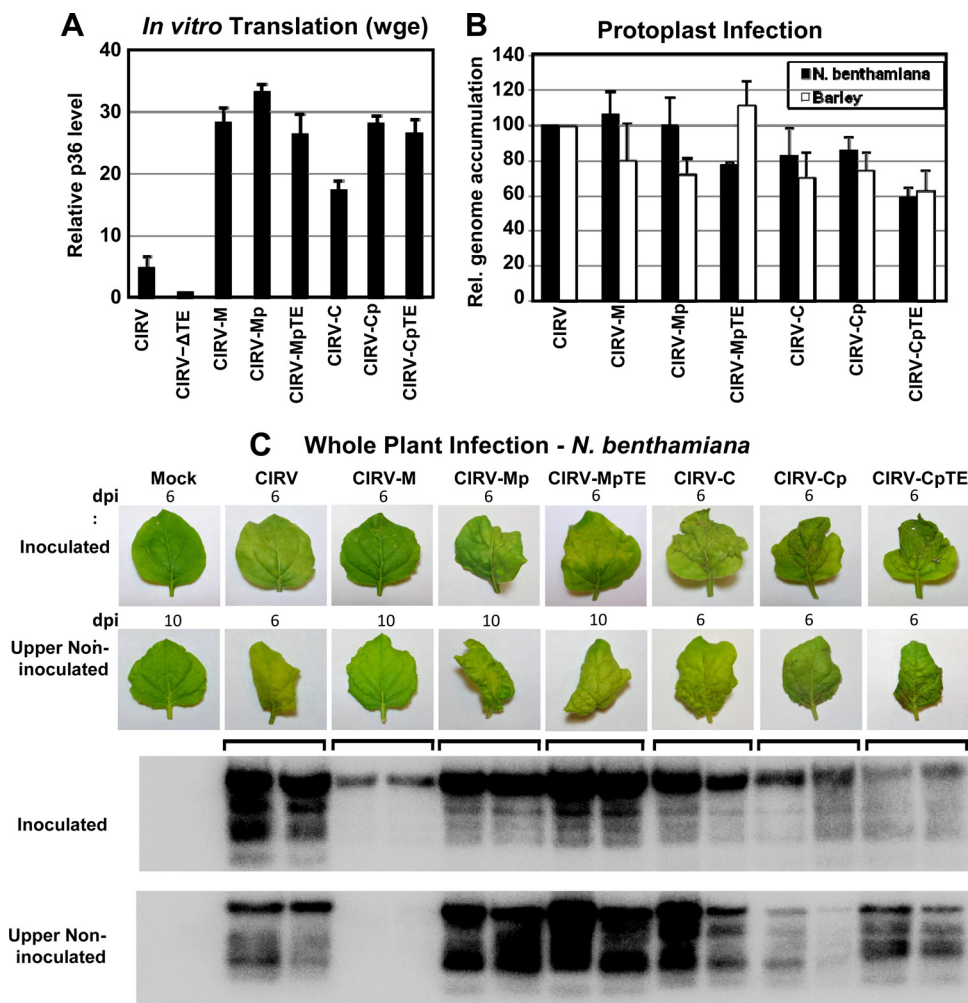


FIG 7 *In vitro* and *in vivo* activities of hybrid CIRV genomes containing 3'CITE mutations obtained during serial passage. (A) Graphical representation of p36 accumulation in wge translation reactions. The relative levels of p36 produced from the RNAs identified below the graph were normalized to the level seen with CIRV-ΔTE (set to 1). (B) Accumulation of viral genomic RNAs in *N. benthamiana* and barley protoplasts (analyzed by Northern blotting). (C) Upper panel: inoculated leaves at 6 dpi and upper noninoculated leaves at 6 dpi (for CIRV, CIRV-C, CIRV-Cp, and CIRV-CpTE) or 10 dpi (for mock treatment, CIRV-M, CIRV-Mp, and CIRV-MpTE). Lower panel: Northern blot showing viral RNA accumulation in leaves from two plants inoculated with the RNAs indicated above the photographs. Leaves shown are representative of all plants inoculated with the indicated genome over three separate experiments. In each trial, two plants were inoculated with each genome.

genome. At this position distal to the 5'UTR, the eIFs would likely be ineffective at recruiting the small subunit of the ribosome to the 5' end. However, our previous results demonstrated the requirement for an RNA-RNA interaction between the 5'UTR and 3'CITE in CIRV for efficient 3'CITE-mediated translation (21). Therefore, as has been proposed for other 3'CITEs such as the BTE and I-shape 3'CITE (17, 24), the CIRV 3'CITE-bound eIFs may be relocated to the 5' end of the genome via a long-range RNA-RNA interaction. The fact that the TBSV 3'CITE also binds to eIFs (Fig. 3C) and requires a similar 5'UTR-3'CITE interaction for function (19, 20) suggests that this general mechanism also applies to other Y-shaped 3'CITEs in tombusviruses.

3'CITE-genome compatibility. On the basis of the presence of different 3'CITEs in members of the same genus and the existence of the same type of 3'CITE in different genera, we sought to gain a better understanding of 3'CITE-genome compatibility using CIRV as a model. Both the I-shaped and PTE 3'CITEs were effi-

cient mediators of CIRV translation in place of the wt Y-shaped element. This is consistent with an evolutionary model in which 3'CITEs can be exchanged between viruses as modular translational enhancer elements via recombination. The fact that CIRV was fully functional with heterologous 3'CITEs suggests that there is no 3'CITE type-specific regulatory mechanism required to coordinate translation with genome replication. Such coordination has been proposed to be involved in another translational event in CIRV, namely, the translational readthrough of p36 that generates the p95 polymerase (42). Although CIRV may not require a specific 3'CITE to coordinate translation and genome replication, a common mechanistic feature shared by all three of these 3'CITEs (i.e., the essential 5'UTR-3'CITE RNA-RNA interaction) could allow for a general regulatory mechanism. In this model, first proposed by the Miller group, translation would be downregulated by disruption of the 5'-3' RNA-RNA interaction by the viral polymerase during copying of the genome (43). This would free the

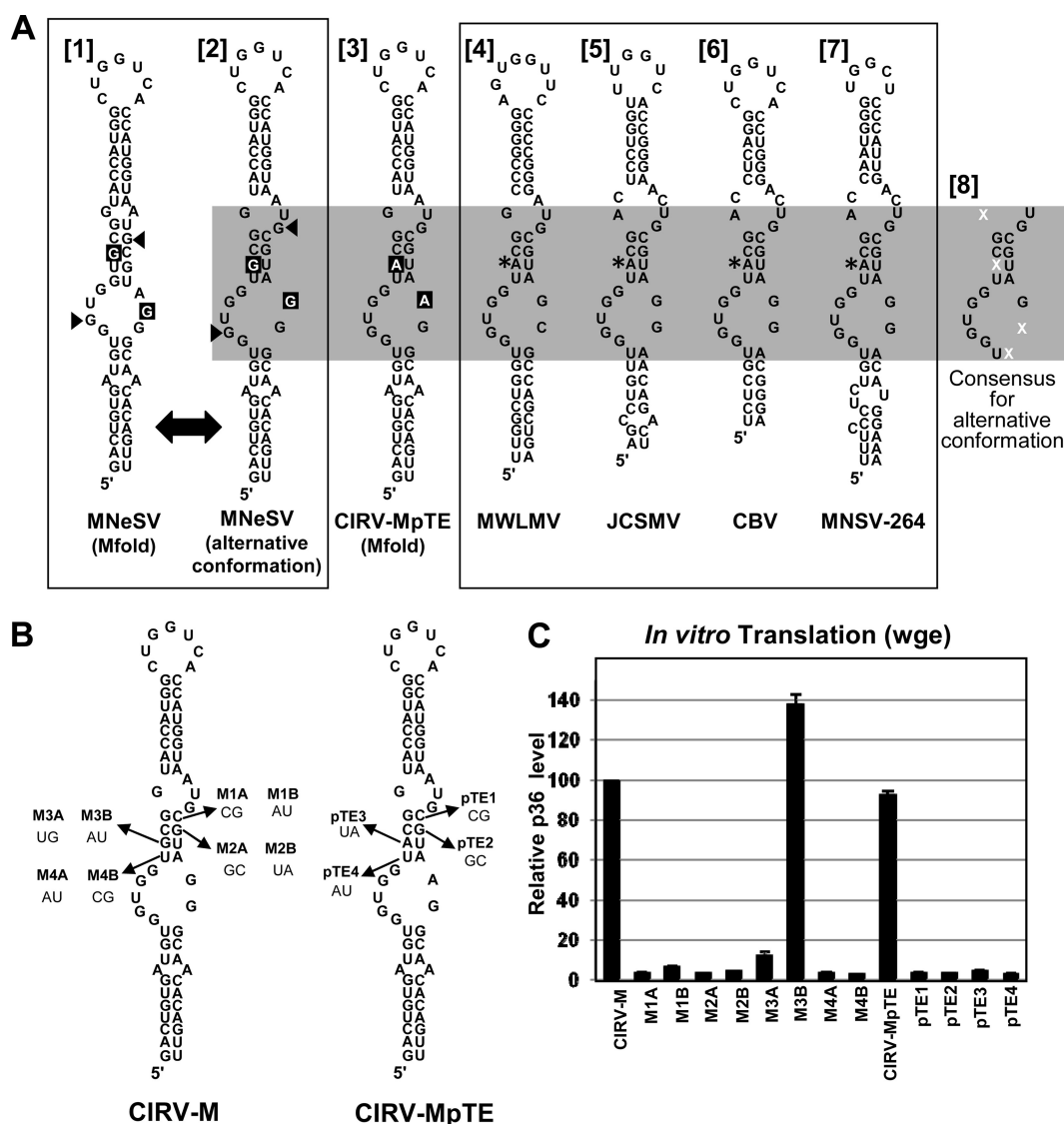


FIG 8 A possible alternative consensus secondary structure for the I-shaped 3'CITE. (A) Comparison of the I-shaped 3'CITEs of different viruses. The Mfold-predicted [1] and alternative [2] secondary structures of the wt MNeSV 3'CITE are depicted in the left-hand box. The small arrowheads indicate residues that were previously found to be highly flexible by solution structure mapping (17). The two guanine residues that were substituted with adenines during serial passage (present in CIRV-MpTE and depicted in structure [3]) are shown in white text on a black background. I-shaped 3'CITEs naturally occurring in other viruses are shown in the right-hand box (structures [4] to [7]) and are depicted in the alternative secondary structure conformation. Asterisks denote a conserved adenine residue that is not maintained in MNeSV (compare to structure [2]). The gray rectangle highlights the previously defined core consensus region of the I-shaped 3'CITE, with the consensus sequence specified in structure [8]. Nucleotides represented by a white "X" are not defined in the consensus sequence. (B) Mutations made to the alternative structure four-base central stem in CIRV-M and CIRV-MpTE, as indicated. For each mutant, the targeted base pair is indicated by an arrow, and the mutations made are shown with mutant names above in bold. (C) Relative p36 accumulation in wge translation reaction mixtures containing RNA transcripts of the mutants named below the graph. p36 levels were normalized to CIRV-M, which was set to 100.

genome of ribosomes so that minus-strand synthesis could occur unimpeded. For other viruses, such as *Turnip crinkle virus*, a 3'CITE type-specific regulatory mechanism may indeed be involved in coordinating translation and genome replication, because its 3'CITE is also a replication element (44).

Compatibility of the I-shaped and PTE 3'CITEs with the CIRV genome may be related to similarities in function between these elements and the wt Y-shaped 3'CITE, such as eIF4F recruitment and 3'CITE-5'UTR base pairing. In contrast, the BTE was inactive in the CIRV genome in all assays used in this study. The source of incompatibility is unclear, but one difference is that the BTE tested

in CIRV may not function via a 5'UTR-3'CITE long-range RNA-RNA interaction in its native context of TNV-D (13). Therefore, attempts to compel it to do so within the CIRV genome may have been ineffective. Additionally, the wt TNV-D BTE 3'-adapter loop is sensitive to sequence changes (13); thus, another possibility is that the altered 3'-adapter loop that was introduced into the BTE in CIRV-T (Fig. 1E) inhibited BTE function. To test this possibility, we engineered and tested a CIRV-T genome containing the wt TNV-D BTE with a wt 3'-adapter loop (which still maintains some complementarity with the CIRV 5' adapter [Fig. 1A and E]) and found it too to be nonfunctional in all assays (data not

shown), suggesting that there is indeed an incompatibility between CIRV and this BTE.

Effects of the 3'CITE on viral infectivity in plants. While CIRV-M and CIRV-C performed relatively efficiently in *in vitro* translation and *N. benthamiana* protoplast assays, there was a considerable difference in the infections they produced in *N. benthamiana* plants (Fig. 5). CIRV-M caused only limited local infections and was not able to spread systemically, while CIRV-C accumulated to high levels and caused rapid generalized necrosis (Fig. 5). The small replicative advantage seen for CIRV-C in the *N. benthamiana* protoplast infections (Fig. 4B) may have provided this virus with enhanced fitness that allowed it to effectively compete at the whole-plant level. The disparate effects of CIRV-M and CIRV-C in *N. benthamiana* plants indicate that the type of 3'CITE can significantly influence virus infectivity and symptomology. In terms of viral exchange of 3'CITEs via recombination in nature, these results highlight the fact that, in addition to being compatible with its new genomic context, a heterologous 3'CITE must also be effective enough to produce sufficient quantities of viral proteins to establish an infection and allow spread within the host plant. This notion is underscored by the observation that, although wt CIRV, CIRV-M, and CIRV-C readily replicated in barley protoplasts, none was able to infect barley plants. Therefore, although the wt and heterologous 3'CITEs are clearly compatible with the cellular barley translation system, other features of these chimeric viruses (e.g., movement protein or suppressor protein) must render them incompatible with whole-plant infections. However, it is possible that this observation is not related to the chimeric nature of these viruses, since plant viruses can often infect nonhost protoplasts while being unable to infect the corresponding whole plants.

Mechanistic insights from 3'CITE passages in plants. Our whole-plant infection data demonstrate that changing the type of 3'CITE or the structure of a specific 3'CITE can have a considerable effect on infectivity in *N. benthamiana*. The latter finding is consistent with host compatibility studies carried out with the carmovirus *Melon necrotic spot virus* (MNSV), which harbors an I-shaped 3'CITE (18, 45). For MNSV, it was found that the I-shaped 3'CITE structure influenced both resistance within melon cultivars and the ability to overcome nonhost resistance in *N. benthamiana* (18, 46). In our case, we observed that the two single-nucleotide substitutions in the I-shaped 3'CITE obtained during serial passage of CIRV-M were sufficient to cause a major enhancement of infectivity, movement, and symptoms in *N. benthamiana* (Fig. 7C). Collectively, these results complement and reinforce the concept of I-shaped 3'CITEs as determinants of systemic movement, host range, and symptomology. The two substitutions identified in the adapted I-shaped 3'CITE enhanced plant but not protoplast infection of *N. benthamiana*, indicating a clear benefit only in a whole-plant context. As such, the advantage could be related to the more optimal translation of movement, coat, and/or suppressor proteins from the two subgenomic (sg) mRNAs produced during infection, all of which play important roles in whole-plant infections. The two substitutions hinted at a possible common alternative functional structure for the I-shaped 3'CITEs; however, extensive mutagenesis could not confirm this notion (Fig. 8), and thus, the relevant structure(s) of the central core motif remains elusive. One possibility is that the MNeSV 3'CITE requires both structures for function and must maintain the structural flexibility necessary to convert between the two. In

support of this concept, mutations that were predicted to maintain the original structure or the alternative structure (but not both) inhibited 3'CITE activity (Fig. 8B) (17). However, mutants M1B and M2B (Fig. 8B) are predicted to support formation of both conformations but are also nonfunctional, suggesting that if two structures are required, sequence identity is still important. Indeed, the sequence identity of the core region of the I-shaped 3'CITE is highly conserved (Fig. 8A), and the major exception to the consensus is an A-to-G substitution in MNeSV that is amenable to formation of both structures (Fig. 8A [1] and [2]). Another possibility is that the relevant conformation of the I-shaped 3'CITE involves higher-order or noncanonical interactions that cannot be predicted.

ACKNOWLEDGMENTS

We thank members of our laboratory for reviewing the manuscript.

B.L.N. is supported by an NSERC Canada Graduate Scholarship. This research was supported by grants from the National Science Foundation to K.S.B. (MCB1052530 and Arabidopsis 2010 S-0000335) and from NSERC, CFI, and CRC to K.A.W.

REFERENCES

- Gallie DR. 1991. The cap and poly(A) tail function synergistically to regulate mRNA translation efficiency. *Genes Dev.* 5:2108–2116.
- Gingras AC, Raught B, Sonenberg N. 1999. eIF4 initiation factors: effectors of mRNA recruitment to ribosomes and regulators of translation. *Annu. Rev. Biochem.* 68:913–963.
- Imataka H, Gradi A, Sonenberg N. 1998. A newly identified N-terminal amino acid sequence of human eIF4G binds poly(A)-binding protein and functions in poly(A)-dependent translation. *EMBO J.* 17:7480–7489.
- Gallie DR. 1998. A tale of two termini: a functional interaction between the termini of an mRNA is a prerequisite for efficient translation initiation. *Gene* 216:1–11.
- Gallie DR. 2002. Protein-protein interactions required during translation. *Plant Mol. Biol.* 50:949–970.
- Browning KS, Webster C, Roberts JK, Ravel JM. 1992. Identification of an isozyme form of protein synthesis initiation factor 4F in plants. *J. Biol. Chem.* 267:10096–10100.
- Dreher TW, Miller WA. 2006. Translational control in positive strand RNA plant viruses. *Virology* 344:185–197.
- Miller WA, Wang Z, Treder K. 2007. The amazing diversity of cap-independent translation elements in the 3'-untranslated regions of plant viral RNAs. *Biochem. Soc. Trans.* 35:1629–1633.
- Nicholson BL, White KA. 2011. 3' cap-independent translation enhancers of positive-strand RNA plant viruses. *Curr. Opin. Virol.* 1:373–380.
- Wang S, Miller WA. 1995. A sequence located 4.5 to 5 kilobases from the 5' end of the barley yellow dwarf virus (PAV) genome strongly stimulates translation of uncapped mRNA. *J. Biol. Chem.* 270:13446–13452.
- Salem NM, Miller WA, Rowhani A, Golino DA, Moyne AL, Falk BW. 2008. Rose spring dwarf-associated virus has RNA structural and gene-expression features like those of Barley yellow dwarf virus. *Virology* 375:354–360.
- Wang Z, Kraft JJ, Huim A, Miller WA. 2010. Structural plasticity of Barley yellow dwarf virus-like cap-independent translation elements in four genera of plant viral RNAs. *Virology* 402:177–186.
- Shen R, Miller WA. 2004. The 3' untranslated region of tobacco necrosis virus RNA contains a barley yellow dwarf virus-like cap-independent translation element. *J. Virol.* 78:4655–4664.
- Batten JS, Desvoves B, Yamamura Y, Scholthof KB. 2006. A translational enhancer element on the 3'-proximal end of the Panicum mosaic virus genome. *FEBS Lett.* 580:2591–2597.
- Wang Z, Parisien M, Scheets K, Miller WA. 2011. The cap-binding translation initiation factor, eIF4E, binds a pseudoknot in a viral cap-independent translation element. *Structure* 19:868–880.
- Scheets K, Redinbaugh MG. 2006. Infectious cDNA transcripts of Maize necrotic streak virus: infectivity and translational characteristics. *Virology* 350:171–183.
- Nicholson BL, Wu B, Chevtchenko I, White KA. 2010. Tombusvirus

- recruitment of host translational machinery via the 3' UTR. *RNA* 16: 1402–1419.
18. Truniger V, Nieto C, González-Ibeas D, Aranda M. 2008. Mechanism of plant eIF4E-mediated resistance against a Carmovirus (Tombusviridae): cap-independent translation of a viral RNA controlled in cis by an (a)virulence determinant. *Plant J.* 56:716–727.
 19. Fabian MR, White KA. 2004. 5'-3' RNA-RNA interaction facilitates cap- and poly(A) tail-independent translation of tomato bushy stunt virus mRNA: a potential common mechanism for tombusviridae. *J. Biol. Chem.* 279:28862–28872.
 20. Fabian MR, White KA. 2006. Analysis of a 3'-translation enhancer in a tombusvirus: a dynamic model for RNA-RNA interactions of mRNA termini. *RNA* 12:1304–1314.
 21. Nicholson BL, White KA. 2008. Context-influenced cap-independent translation of Tombusvirus mRNAs in vitro. *Virology* 380:203–212.
 22. Treder K, Kneller EL, Allen EM, Wang Z, Browning KS, Miller WA. 2008. The 3' cap-independent translation element of Barley yellow dwarf virus binds eIF4F via the eIF4G subunit to initiate translation. *RNA* 14: 134–147.
 23. Wang Z, Treder K, Miller WA. 2009. Structure of a viral cap-independent translation element that functions via high affinity binding to the eIF4E subunit of eIF4F. *J. Biol. Chem.* 284:14189–14202.
 24. Guo L, Allen EM, Miller WA. 2001. Base-pairing between untranslated regions facilitates translation of uncapped, nonpolyadenylated viral RNA. *Mol. Cell* 7:1103–1109.
 25. Chattopadhyay M, Shi K, Yuan X, Simon AE. 2011. Long-distance kissing loop interactions between a 3' proximal Y-shaped structure and apical loops of 5' hairpins enhance translation of Saguaro cactus virus. *Virology* 417:113–125.
 26. Rakotondrafara AM, Polacek C, Harris E, Miller WA. 2006. Oscillating kissing stem-loop interactions mediate 5' scanning-dependent translation by a viral 3'-cap-independent translation element. *RNA* 12:1893–1906.
 27. Stupina VA, Meskauskas A, McCormack JC, Yingling YG, Shapiro BA, Dinman JD, Simon AE. 2008. The 3' proximal translational enhancer of Turnip crinkle virus binds to 60S ribosomal subunits. *RNA* 14:2379–2393.
 28. Stupina VA, Yuan X, Meskauskas A, Dinman JD, Simon AE. 2011. Ribosome binding to a 5' translational enhancer is altered in the presence of the 3' untranslated region in cap-independent translation of turnip crinkle virus. *J. Virol.* 85:4638–4653.
 29. Sztuba-Solińska J, Urbanowicz A, Figlerowicz M, Bujarski JJ. 2011. RNA-RNA recombination in plant virus replication and evolution. *Annu. Rev. Phytopathol.* 49:415–443.
 30. Mathews DH, Sabina J, Zuker M, Turner DH. 1999. Expanded sequence dependence of thermodynamic parameters provides robust prediction of RNA secondary structure. *J. Mol. Biol.* 288:911–940.
 31. Zuker M. 2003. Mfold web server for nucleic acid folding and hybridization prediction. *Nucleic Acids Res.* 31:3406–3415.
 32. Burgyn J, Rubino L, Russo M. 1996. The 5'-terminal region of a tombusvirus genome determines the origin of multivesicular bodies. *J. Gen. Virol.* 77:1967–1974.
 33. Sambrook J, Fritsch EF, Maniatis T. 1989. *Molecular cloning: a laboratory manual*, 2nd ed. Cold Spring Harbor Laboratory Press, Cold Spring Harbor, NY.
 34. Dangerfield JA, Windbichler N, Salmons B, Gunzberg WH, Schroder R. 2006. Enhancement of the StreptoTag method for isolation of endogenously expressed proteins with complex RNA binding targets. *Electrophoresis* 27:1874–1877.
 35. White KA, Morris TJ. 1994. Nonhomologous RNA recombination in tombusviruses: generation and evolution of defective interfering RNAs by stepwise deletions. *J. Virol.* 68:14–24.
 36. Mayberry LK, Dennis MD, Allen ML, Ruud Nitka K, Murphy PA, Campbell L, Browning KS. 2007. Expression and purification of recombinant wheat translation initiation factors eIF1, eIF1A, eIF4A, eIF4B, eIF4F, eIF(iso)4F, and eIF5. *Methods Enzymol.* 430:397–408.
 37. Gallie DR. 2007. Use of in vitro translation extract depleted in specific initiation factors for the investigation of translational regulation. *Methods Enzymol.* 429:35–51.
 38. Windbichler N, Schroeder R. 2006. Isolation of specific RNA-binding proteins using the streptomycin-binding RNA aptamer. *Nat. Protoc.* 1:637–640.
 39. Gazo BM, Murphy P, Gatchel JR, Browning KS. 2004. A novel interaction of Cap-binding protein complexes eukaryotic initiation factor (eIF) 4F and eIF(iso)4F with a region in the 3'-untranslated region of satellite tobacco necrosis virus. *J. Biol. Chem.* 279:13584–13592.
 40. Wu B, White KA. 1999. A primary determinant of cap-independent translation is located in the 3'-proximal region of the tomato bushy stunt virus genome. *J. Virol.* 73:8982–8988.
 41. Iwakawa HO, Tajima Y, Taniguchi T, Kaido M, Mise K, Tomari Y, Taniguchi H, Okuno T. 2012. Poly(A)-binding protein facilitates translation of an uncapped/nonpolyadenylated viral RNA by binding to the 3' untranslated region. *J. Virol.* 86:7836–7849.
 42. Cimino PA, Nicholson BL, Wu B, Xu W, White KA. 2011. Multifaceted regulation of translational readthrough by RNA replication elements in a tombusvirus. *PLoS Pathog.* 7:e1002423. doi:10.1371/journal.ppat.1002423.
 43. Barry JK, Miller WA. 2002. A -1 ribosomal frameshift element that requires base pairing across four kilobases suggests a mechanism of regulating ribosome and replicase traffic on a viral RNA. *Proc. Natl. Acad. Sci. U. S. A.* 99:11133–11138.
 44. Yuan X, Shi K, Meskauskas A, Simon AE. 2009. The 3' end of Turnip crinkle virus contains a highly interactive structure including a translational enhancer that is disrupted by binding to the RNA-dependent RNA polymerase. *RNA* 15:1849–1864.
 45. Nieto C, Morales M, Orjeda G, Clepet C, Monfort A, Sturbois B, Puigdomènech P, Pitrat M, Caboche M, Dogimont C, García-Mas J, Aranda MA, Bendahmane A. 2006. An eIF4E allele confers resistance to an uncapped and non-polyadenylated RNA virus in melon. *Plant J.* 48: 452–462.
 46. Nieto C, Rodríguez-Moreno L, Rodríguez-Hernández AM, Aranda MA, Truniger V. 2011. *Nicotiana benthamiana* resistance to non-adapted *Melon necrotic spot virus* results from an incompatible interaction between virus RNA and translation initiation factor 4E. *Plant J.* 66:492–501.